



This is the accepted manuscript made available via CHORUS. The article has been published as:

Percolation and dissolution of Borromean networks

Donald G. Ferschweiler, Ryan Blair, and Alexander R. Klotz

Phys. Rev. E **107**, 024304 — Published 7 February 2023

DOI: [10.1103/PhysRevE.107.024304](https://doi.org/10.1103/PhysRevE.107.024304)

Percolation and Dissolution of Borromean Networks

Donald G. Ferschweiler,¹ Ryan Blair,² and Alexander R. Klotz^{a1}

¹*Department of Physics and Astronomy, California State University, Long Beach*

²*Department of Mathematics and Statistics, California State University, Long Beach*

Inspired by experiments on topologically linked DNA networks, we consider the connectivity of Borromean networks, in which no two rings share a pairwise-link, but groups of three rings form inseparable triplets. Specifically, we focus on square lattices at which each node is embedded a loop which forms a Borromean link with pairs of its nearest neighbors. By mapping the Borromean link network onto a lattice representation, we investigate the percolation threshold of these networks, (the fraction of occupied nodes required for a giant component), as well as the dissolution properties: the spectrum of topological links that would be released if the network were dissolved to varying degrees. We find that the percolation threshold of the Borromean square lattice occurs when approximately 60.75% of nodes are occupied, slightly higher than the 59.27% typical of a square lattice. Compared to the dissolution of Hopf-linked networks, a dissolved Borromean network will yield more isolated loops, and fewer isolated triplets per single loop. Our simulation results may be used to predict experiments from Borromean structures produced by synthetic chemistry.

INTRODUCTION

Mechanically interlocked molecules such as linked-ring catenanes and shish-kebab rotaxanes have chemical components that are non-covalently connected through non-trivial topological linkages [1]. Such molecules have been proposed as the basis for switches and motors for nanoscale machines. One such exotic molecular topology is the Borromean rings, which consist of three mutually entangled loops for which no two loops share a binary entanglement. Borromean rings were originally the heraldic symbol of the House of Borromeo and feature prominently in centuries of art, can be constructed from organometallic synthesis [2] or DNA origami [3], and serve as an analogy for certain bound states in nuclear physics [4].

The framework of mechanically interlocked molecules may be extended to mechanically interlocked networks or lattices, sometimes referred to as molecular chainmail [5]. Space-filling “topological crystals” have been synthesized, using Hopf linking to connect two repeating chemical motifs [6], and disordered space-filling Olympic gels have been created by using enzymes to Hopf link circular DNA molecules [7]. Large, regular, planar structures with Borromean connectivity are referred to as Borromean networks, or Borromean lattices or chainmail, which are depicted with square lattice symmetry in Figure 1. Borromean networks extend the existing concept of the Olympic gel, a network of Hopf-linked molecular rings [8], into a system with only Borromean connectivity. Borromean lattices are not Brunnian in that the removal of a single component may remove several other but will not dissolve the network entirely. Physical Borromean lattices have been created by synthetic chemists [9–12], and the crystallographic symmetry of Borromean lattices has been discussed [13, 14].

As the relationship between molecular topology and bulk material properties become better understood and our ability to synthesize tailored topological crystals improves, it will become necessary to experimentally determine whether the designed topology of a material has been realized. Real-space techniques such as atomic force microscopy and transmission electron microscopy can image these structures at the molecular scale, but it is difficult to map molecules in three dimensions to verify, for example, whether one molecule passes over or under another in order to verify a specific knot topology. Spectroscopic and crystallographic techniques may determine the proximity of individual atoms but do not directly probe topology and are unsuitable for systems that lack rigid crystalline order such as polymer-based topological structures. An assay that can directly probe the topology, rather than the geometry, of a material will be useful when topological chemistry is more widespread.

Although the synthetic capabilities for extended topologically linked molecular structures is relatively recent, such structures occur in nature: the HK97 virus consists of topologically linked proteins forming an icosahedral capsid [16] and kinetoplasts are complex topologically linked networks of DNA molecules found in the mitochondria of trypanosome parasites. Each kinetoplast consists of about 5000 linked DNA “minicircles” which decode the RNA produced by a few dozen linked “maxicircles” [17]. Each minicircle in a kinetoplast is Hopf-linked to its spatial neighbors. The topology of kinetoplast networks is estimated in experiments that dissolve the network using enzymes

^a alex.klotz@csulb.edu

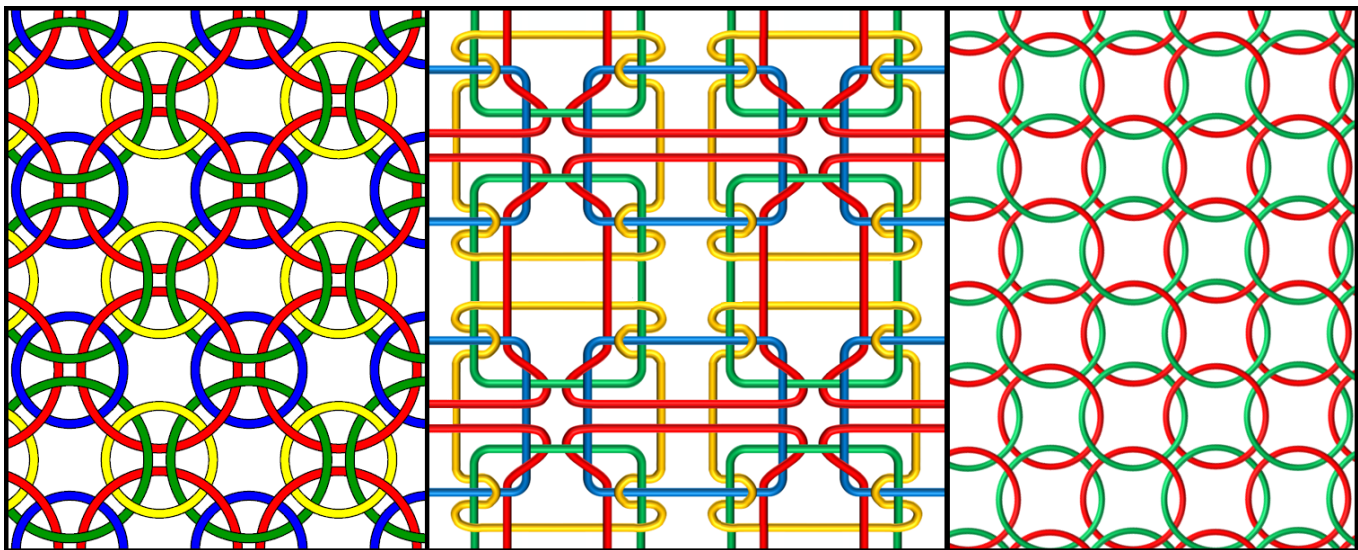


FIG. 1. Left: Stylistic rendering of a Borromean chainmail square lattice by Luc Devroye [15]. No two rings share a direct topological link, but no ring can be removed from the network. Middle: A fully symmetric Borromean lattice, in which any three of the four colored components will remain in Borromean connection if the fourth is removed. This is the primary network of investigation in this study. Right: a traditional Hopf-linked chainmail network with square lattice symmetry.

that break individual minicircles, and measure the relative frequency of different topological structures, the topological spectrum, by gel electrophoresis [18, 19]. The network topology is determined by comparing the relative frequency of different components (the ratio of 2-catenanes to single loops, for example) to the predictions from graph theory models. A similar assay could be developed for solid state catenated materials using mass spectrometry to size the topological links released as a crystal is broken down. Such experiments will only be useful if it is known how a given molecular or crystalline topology will dissolve and what the predicted topological spectrum is. This is known for traditional lattice geometries with pairwise connectivity, and the purpose of this manuscript is extend that knowledge to Borromean connectivity, such that the topology of future materials may be understood.

The electrical and mechanical properties of future topological materials may be modified by the removal of constituent molecules from the networks, in analogy to the modification of two-dimensional material properties by the perforation of molecular sheets [20]. Such modification has recently been demonstrated for kinetoplast DNA, in which the networks were softened by the partial removal of minicircles from the network [21]. Links can only be stochastically removed from a network up to a certain fraction, after which the percolation threshold is exceeded and the network is no longer cohesive. The percolation threshold of most crystal lattices is well established, but such calculations assume pairwise connectivity between nodes, which is not the case for Borromean networks. This work is concerned with estimating the percolation threshold of the Borromean square lattice.

A lattice with regular geometry may be regarded as full if each geometric site on the lattice is occupied by a node in a network or graph that shares edges with its geometric neighbors. A full lattice has a single component that spans the entire length scale of the network, known as the giant connected component. As nodes or edges are removed from the network, smaller clusters will be isolated when none of their nodes share edges with the giant component. If a sufficient fraction of edges or nodes is removed, the largest component in the system will no longer span the length scale of the system, and the giant connected component will cease to exist. The minimum fraction of filled nodes or edges in a graph that allows a giant connected component to exist is known as the percolation threshold [22] and depends on the topology of the graph (for example, a square lattice requires 59.27% of its sites occupied to reach percolation [23]). Systems at the percolation threshold have universal properties (such as a cluster size distribution exponent and a fractal dimension) that depends only on space dimensionality but not graph topology [24].

In this work we aim to develop a means of predicting the results of future experiments on Borromean materials such as those developed by Thorp-Greenwood et al [9]. Through computational graph theory, we will predict topological spectrum and the percolation threshold of Borromean networks with square lattice topology. We compare these results to the dissolution of a traditionally connected graph, which serves as an analogy to Hopf-linked topological lattices like kinetoplast DNA. Although this work is primarily concerned with the mathematical analysis of Borromean networks, it may prove useful in future experiments in determining whether a topological material contains Borromean

or Hopf-linked connectivity.

MODEL AND ALGORITHM

We will first describe the spatial structure of Borromean networks, before introducing a simplifying graph model. Figure 1 depicts three topological networks with square lattice symmetry; the square lattices are recovered if the center of mass of each loop is replaced with a point. The figure on the left is an artistic rendering of Borromean chainmail by Luc Devroye. Readers not familiar with Borromean networks may inspect which colored rings pass over and under each other, verifying that no two rings are connected, but also that no ring may be pulled out from the network. They can picture the effect of, for example, removing the blue rings and seeing that red, green, and yellow still form Borromean links, but that if red is removed then no other color is bound. In this sense, this network does not have full symmetry: different components have different effects when removed from the network. As a historical note, a similar structure with triangular lattice symmetry was drawn in a letter from James Clerk Maxwell to Peter Guthrie Tate [25].

The center diagram has a significantly more complex crossing structure but is fully symmetric: if any color is entirely removed from the network, the other three colored components remain in Borromean linkage with each other. This leads to redundant linking between components and their lattice neighbors. For example, the red hourglass-shaped curve in the middle of the diagram forms Borromean rings with the green to its left and the blue above, with the blue above and the yellow to the top-left, and the green to its left and the yellow to its top left, and forms similar three linkages in the other three quadrants. Each loop is topologically identical as part of twelve Borromean ring triplets. In principle, Reidemeister moves may be used to transform all of one class of components into the shape of another (e.g. the reds and yellows can be smoothed into rectangles at the expense of the greens and blues becoming hourglass shaped), which is not the case for the diagram on the left. While it is more likely that Borromean materials have a simpler structure like that of Devroye, we focus our computations on the fully symmetric case.

The diagram on the right of Figure 1 shows traditional square lattice chainmail (known as 4-in-1 in the armor community), where each ring is Hopf-linked to its four nearest neighbors. Each ring is geometrically and topologically identical, the two colors are used as a visual aid. The connectivity of this Hopf-linked network is exactly the same as that of any square lattice with nearest-neighbor connections, a well-studied system with a known percolation threshold that is used as a comparison to our analysis of the Borromean system.

It is, in principle, possible to generate Cartesian coordinates for a large Borromean network, remove certain components to simulate an incomplete network, and calculate three-body knot invariants [26] between every subset of three loops to determine the overall connectivity. An easier test is possible using the Gauss linking number on a Hopf-linked network. This, however is prohibitively inefficient computationally. Instead, we take advantage of the square lattice, in which every right triangle formed by neighboring loops will share a Borromean linkage. That Borromean links form a 3-hypergraph and can be represented as a closed triangle on a graph was pointed out by Zapata-Carratala and Arsiwalla [27]. We represent topologically linked networks as a square lattices with each node representing an individual loop, similar to Figure 1. With “standard” connectivity rules, two occupied sites on a lattice are considered adjacent (sharing an edge in a graph) if they are orthogonally next to each other. This can be taken as analogous to two loops sharing a Hopf link. Unlike a Hopf-linked network with standard pairwise connectivity, Borromean lattice contains no pairwise adjacency, at least three loops are required to establish connectivity. Instead, we define Borromean connectivity, where groups of three occupied sites are considered mutually adjacent if they form the smallest possible right triangle on the lattice, such that the three loops represented by the appropriate space curves at these sites would form Borromean rings. Nodes that are not part of a triangle share no edges with other nodes.

Our goal is determine the cluster size distribution of incomplete Borromean networks, e.g. with some fraction removed from the square lattice of loops. A cluster is a subset of nodes that form a connected graph with each other (such that a path exists from any node along edges to any other), but not with any other nodes in the network. The size of a cluster is the number of nodes it contains, and the cluster size distribution refers to the relative frequency that a cluster of a certain size occurs.

Figure 2 shows the mapping between a network of Borromeanly-linked rings (a), the square lattice representation (b), and the graph representation (c). The ring network contains a 10-ring component, a 3-ring Borromean component, and three unlinked rings in spatial proximity. On the lattice, each occupied site in the large component can form a right triangle with at least two of its neighbors, as can each component in the Borromean triplet, but the three singlets cannot. In the graph representation, edges are not shared between the unlinked components. Fig. 2d shows the three representations as a single image.

The mapping between ring network, lattice, and graph allows an efficient simulation of incomplete Borromean

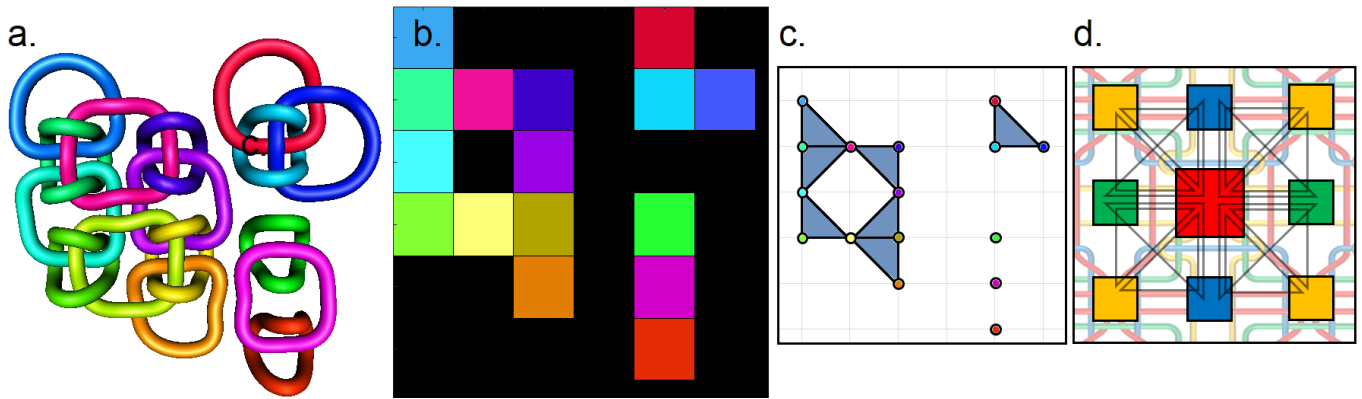


FIG. 2. Mapping between the Borromean lattice and our graph theory representation. a. A Borromean network with a large cluster of ten rings, a triplet of traditional Borromean rings, and three isolated rings. Middle: Representation of the Borromean network on a square lattice where black sites are unoccupied and occupied sites are color-coded with the ring they represent. Right: Graph representation in which each node corresponds to an occupied lattice site, and three nodes share edges if their corresponding lattice sites form a right triangle with unit-length sides, meaning their corresponding rings are Borromeanly linked. d. A portion of the Borromean lattice in Figure 1, with squares at the center of each loop representing lattice sites, and the twelve Borromean connections represented by triangles, showing the three layers of our mapping.

networks. Networks are initialized as random binary matrices of width L representing a square lattice with unoccupied and occupied sites, and can be converted to the 3D representation by substituting a space curve at each lattice site, or converted to the graph representation by calculating which occupied sites form triangles.

Our computations are motivated by experiments that measure the cluster size probabilities of degraded kinetoplasts, and our methods are conceptually similar and involve measuring the cluster sizes of incompletely-filled lattices. To perform our computational measurements, we initialized partially occupied square lattices as random binary matrices, varying the fraction of occupied sites, q , also known as the site occupation probability. We implemented two algorithms to determine the Borromean cluster size distribution based on a binary matrix, and a third to determine the cluster size distribution under Hopf connectivity rules.

Our first algorithm scanned each node of an $N \times N$ binary matrix in a for-loop and checked whether the neighboring nodes required to form each of the twelve triangles were occupied. If they were, three bits were flipped in an $N^2 \times N^2$ binary adjacency matrix, indicating that the three nodes are involved in a Borromean connection, and an additional three were flipped to keep the matrix symmetric under transposition. To distinguish between unoccupied sites and occupied but isolated sites (which would not register on an adjacency matrix), the rows and columns corresponding to empty sites were removed from the adjacency matrix before cluster size calculation.

An adjacency matrix can be converted into a list of clusters by starting with a list containing the first node, checking whether a column in its row of the adjacency matrix is occupied, and if so adding the index of that column to the list. Then, the list of nodes in the cluster is iteratively grown by checking for occupied columns in the rows corresponding to nodes already in the list. When no new nodes are found, a new list for the next cluster is started on the first node not in the first list. This can be made faster by re-ordering the row and column indices of non-zero elements with a reverse Cuthill-McKee algorithm [28, 29] to be located closer to the diagonal. The result of this is a list of clusters, each containing a list of nodes in that cluster.

A lattice with L^2 sites requires an adjacency matrix with L^4 total elements. For larger lattices, the Borromean clustering algorithm becomes computationally unfeasible as the adjacency matrices cannot be accommodated in system memory. Our second algorithm for Borromean lattices builds cluster lists without generating an adjacency matrix. It iterates through each unvisited node, checking a given node for triangular connections with its neighbors and marking the given node as visited in a parallel $N \times N$ matrix. If neighboring nodes share a Borromean connection, those nodes are idempotently added to a growing list of components connected to the original node. The triangular search procedure is repeated for each node that is added to the list, until no more new connections are found. The algorithm then returns to the initial outer iteration and repeats the connected component search for the next unvisited node. This avoids the need for a large adjacency matrix, and is faster on a laptop than our first algorithm for full lattices above $L \approx 50$ and percolating lattices above $L \approx 200$.

The third algorithm, for traditional square lattice connectivity, representing Hopf-link connections, a graphics processing algorithm that uses a flood-fill technique exists to quickly determine connected components (“bwconncomp”

in MATLAB), which is asymptotically faster than the adjacency matrix cluster calculation used for the Borromean lattices. In practice, the Borromean calculations can be sped up by first finding the components with the traditional Hopf connectivity rule, then creating a sub-matrix of each square component and applying the Borromean clustering algorithm to it. At percolation, where the largest cluster size is $\approx 0.45 \times L^{1.9}$, this reduces the memory requirements for the adjacency matrix from L^4 down to roughly $0.2 \times L^{3.8}$.

MATLAB scripts that implement these algorithms may be found at <https://github.com/ramenbytes/borro>.

Our computations are motivated by experiments that measure the cluster size probabilities of degraded kinetoplasts, and our methods are conceptually similar and involve measuring the cluster sizes of incompletely-filled lattices. To perform our computational measurements, we initialized partially occupied square lattices as random binary matrices, varying the fraction of occupied sites, q , also known as the site occupation probability. We calculated the cluster size distribution for Borromean and Hopf connectivity rules from size $L = 12$ up to $L = 1000$. Our algorithms were implemented in MATLAB, and periodic boundary conditions were not used.

The knot-lattice-graph mapping and algorithm in which each node may be Borromean linked in various ways with its eight lattice neighbors represents a fully symmetric square lattice with Borromean connectivity. This corresponds to the network in Figure 1b. The network in Figure 1a allows an easier visualization of the Borromean connectivity, but each blue and yellow component is only Borromean linked with their neighboring green or red components, such that the removal of all the red components would result in the yellow components no longer being connected. We primarily explore the fully symmetric lattice, but discuss results for Devroye’s lattice in the Appendix.

RESULTS AND DISCUSSION

Identifying the Percolation Threshold

Above the percolation threshold, almost all occupied lattice nodes are within the largest cluster, while below the threshold almost none are. The sharpness of this transition increases with the size of the lattice. The size of the second-largest cluster is maximized at the percolation threshold [30], which is our primary method of determining it from our computations. Figure 3 shows the largest and second largest cluster sizes as a function of the occupation probability for Borromean and Hopf-linked square lattices of width $L = 400$. The largest component size varies with occupation probability as expected, with the jump associated with percolation occurring at a higher occupation probability for the Borromean lattice. Examining the second largest component provides more evidence that the Borromean lattice has a higher percolation threshold. We observe that the standard square lattice has a second-largest component that is maximized near the expected value of 0.5927 [23]. Under Borromean connectivity rules, the percolation threshold is slightly but significantly higher. It is difficult to precisely locate the peak with finite numerical precision and a finite-sized lattice, but we estimate the peak at approximately 0.606. A more precise analysis of a regularly-connected square lattice at $L = 400$ finds a second-largest component peak at $q = 0.5917$, 0.16% below the asymptotic value, suggesting that the Borromean percolation threshold is slightly higher than 0.606. Analysis based on the size-independence of the ratio of the two biggest clusters, and the universality of the fractal dimension at percolation (below) puts our estimate at 0.6075.

At the percolation threshold, the ratio of the second largest cluster to the largest cluster is independent of the system size [31–33]. This quantity generally decreases with increasing occupation probability as more and more of the occupied nodes are found in the largest cluster. Below the percolation threshold, larger systems have a larger second-to-first ratio than smaller systems, but above the percolation threshold, smaller systems will have a larger ratio. At the percolation threshold, the ratio is independent of system size. Figure 4 shows this ratio for the Hopf and Borromean square lattices at $N=50, 100,$ and 200 . For the Hopf-connected system, each system has a common second-to-first ratio close to the expected value of 0.5927. The Borromean systems converge on a similar ratio, approximately 0.38, but at an occupation probability between 0.6067 and 0.6078, consistent with the measurement of the second-largest cluster size. **Networks of size $N=400$ were simulated at a finer range of occupation probabilities and weighted linear fits to the $N=50$ and $N=400$ data were performed to find their intersection and its uncertainty. From this we arrive at a percolation threshold of $.60748 \pm 0.00005$. This method of detecting the percolation threshold requires higher precision; in Figure 3b the peak in the second largest cluster could be identified with 80 unique lattices per site, whereas finding the size-independence point requires over 1000.**

The higher occupation ratio required for percolation with Borromean connectivity is illustrated in Figure 5. The largest cluster at the square lattice percolation threshold will span the entire system (in this case defined as touching the four edges of the lattice), but consist of regions where the cluster forms “bridges” only one site wide and several sites long. These can be seen at the green-yellow boundaries in Figure 5. Under the Borromean connectivity rule, the giant

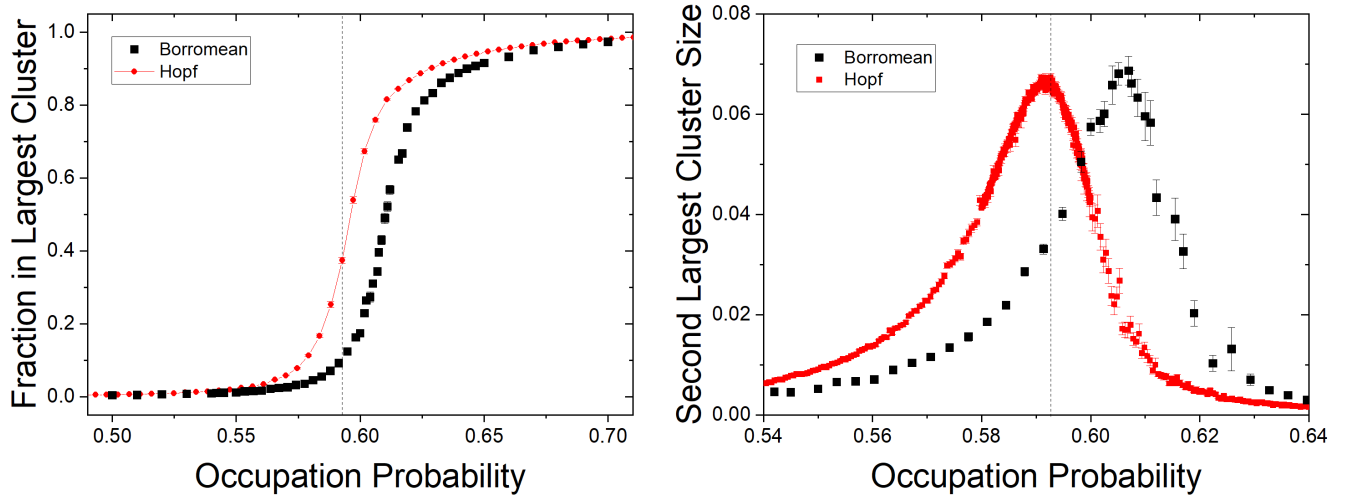


FIG. 3. Left: Fraction of occupied sites in a 400×400 square lattice that are within the largest component, as a function of fraction of sites that are occupied, for the Hopf and Borromean connectivity rules. Right: The second largest component sizes from the same data. The peak of the second largest component indicates the location of the percolation threshold, which is slightly higher for Borromean lattices. In both charts, error bars represent standard error over multiple randomized lattice instances and the established square lattice percolation threshold of 0.5927 is shown by a dashed line.

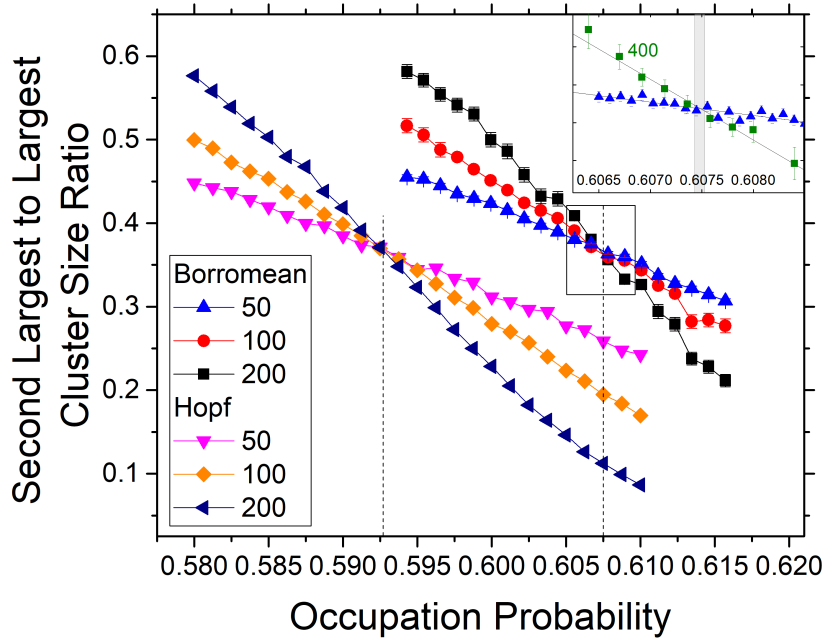


FIG. 4. Ratio of second largest to largest cluster size for Hopf and Borromean square lattices of size 50, 100, and 200 near the percolation threshold. The size dependence of the ratio vanishes at the percolation threshold. The Hopf data converges near the expected value of 0.5927, while size dependence for the Borromean lattice vanishes between 0.6067 and 0.6078. The inset shows higher-resolution data from size 50 and 400 Borromean lattices and their linear fits, indicating a percolation threshold of 0.60748 ± 0.00005 .

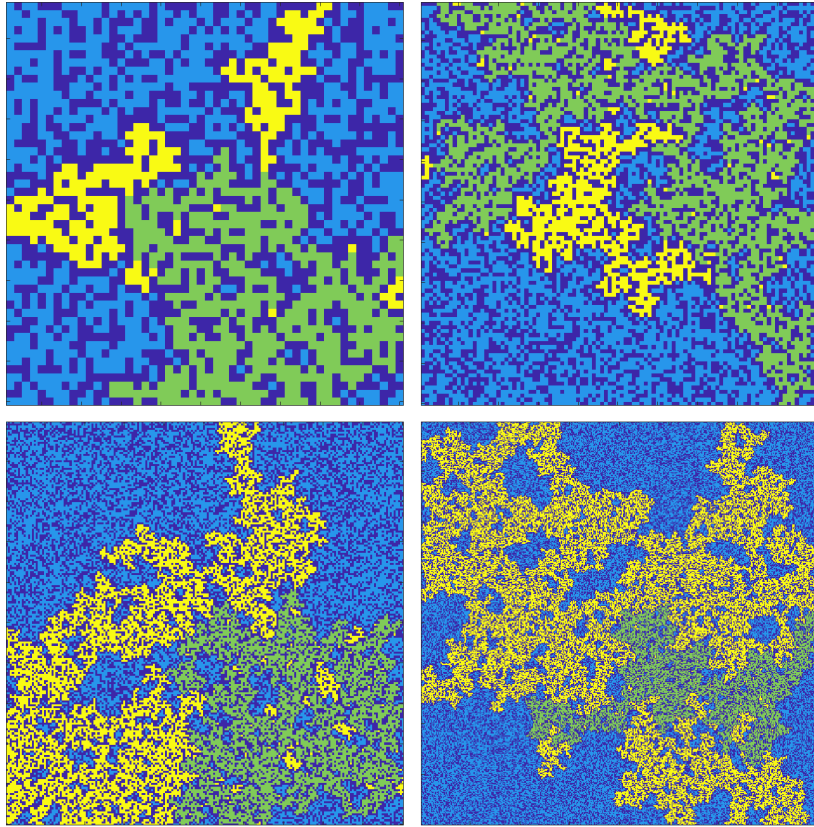


FIG. 5. Square lattices of sizes 50, 100, 200 and 400 with an occupation probability of 0.5927. Dark blue sites are unoccupied and light blue sites are occupied. The largest component under Hopf connectivity rules is shown as the union of the yellow and green sites, and in each case spans the system by touching all four sides. The largest component under Borromean connectivity rules is green, and does not span the system. At the interface of the green and yellow sites are bridges that are connected by Hopf adjacency rules but not Borromean connectivity rules, best seen in the $N=50$ lattice.

cluster does not span these bridges, and forms additional smaller Borromean clusters. Extra occupied sites adjacent to these bridges are required to keep them in the giant cluster, which is why a slightly higher occupation is required for a Borromean network to percolate. Another argument, put forth by Robert Ziff in a personal communication, is as follows: at the square lattice percolation threshold of $q_S = 0.5927$, the probability that two adjacent sites are filled (and form a cluster) is $q_S^2 = 0.3513$. However, for the sites to form a Borromean triplet, one of the four sites adjacent to the doublet must be occupied, which occurs with probability $q^2(1 - (1 - q)^4)$. If we assume that the two-node cluster formation probability on a square lattice must equal 0.3513, q_B must have a value of 0.6004, slightly higher than 0.5927 but slightly slower than what we observe.

Results from the modified connectivity rules that describe the network in Figure 1a are presented in the Appendix. We note that the difference between Borromean and Hopf connectivity in that case is much stronger, and the percolation threshold is located at approximately 0.66.

Universal Behavior

Although the connectivity of the Borromean lattice is not pairwise, it is still local, and at percolation is expected to obey the expected universal behavior of percolating systems. In two dimensions, this includes a fractal dimension for largest cluster size of $91/48 \approx 1.89$ [34], and a cluster size distribution that decays with a $-187/91 \approx 2.05$ power law [35]. The largest component size at $q = 0.6075$ is plot against the system size in Figure 5, along with data for the Hopf lattice at 0.5927, which is essentially identical. The best fit value for the fractal dimension is 1.893 ± 0.002 , or $(90.9 \pm 0.1)/48$. If the largest cluster size from systems that are not at the percolation threshold is examined, it is expected to slightly deviate from power-law behavior, and display a best-fit exponent that is not the universal value. At $q = 0.606$, we observed an exponent of 1.82 ± 0.02 , and at 0.609 we observed 1.96 ± 0.02 . We interpret this

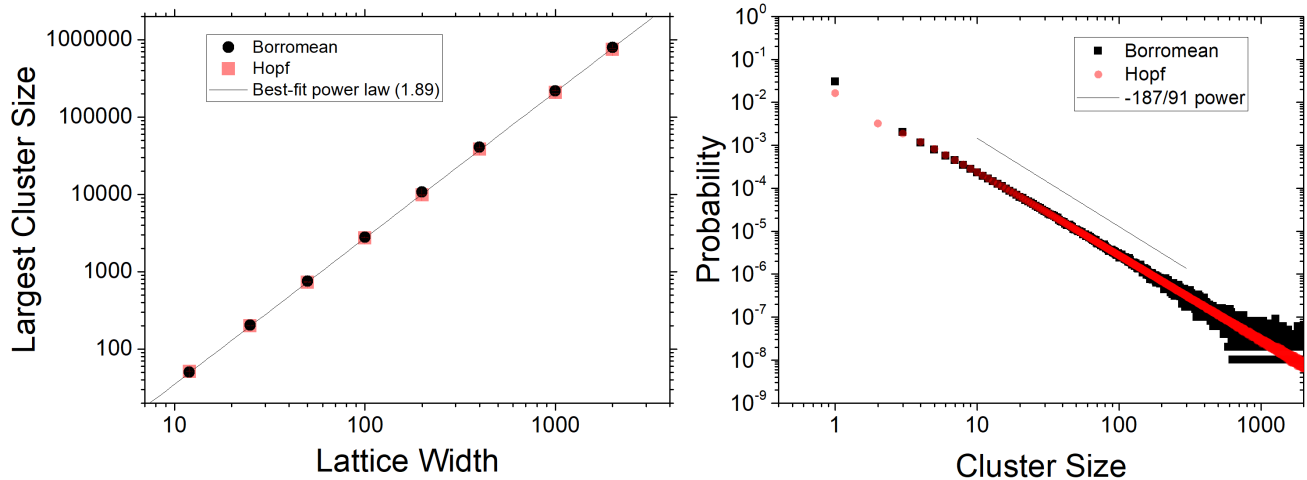


FIG. 6. Universal properties of the percolation threshold. Left: The largest component size as a function of the lattice width for Borromean lattices at $q = 0.6075$, with a best-fit exponent of 1.893 ± 0.002 , consistent with a fractal dimension of $91/48$. Data for regular square connectivity at $q = 0.5927$ is overlaid and effectively identical. Error bars are smaller than points. Right: Cluster size probability distribution for 1000×1000 lattices with Borromean and Hopf connectivity at their respective percolation thresholds. Both distributions are consistent with each other, although presumably due to finite-size effects have a weaker decay exponent than the expected $-187/91$. The Hopf data is more precise due to the faster algorithm used to generate it.

as additional evidence that the percolation threshold of the Borromean square lattice is at approximately 0.6075.

The cluster size distribution at percolation is seen in Figure 6 for both Borromean and Hopf connectivity rules. The distribution is slightly different for the smallest clusters, notably due to the lack of Borromean dimers, but they converge to a similar form for large clusters. We measure best-fit exponents for these distributions as -1.883 ± 0.001 for Borromean and -1.906 ± 0.001 for Hopf connectivity, inconsistent with the Fisher exponent of $-187/91$. The cluster size distribution exponent is more sensitive to finite-size effects: Ding et al. observed a power-law consistent with a -1.92 exponent on square lattices 1000 sites wide [36], while in an earlier study Hoshen et al. observed data consistent with a -1.78 exponent on triangular lattices 4000 sites wide [37]. Only on lattices 2 million sites wide have precise data consistent with the -2.05 exponent been observed [35]. Although finite-size effects persist, we find that Borromean lattices at the percolation threshold display the same universal properties as those with traditional connectivity.

Dissolution Spectrum

An experiment to determine the topology of a hypothetical Borromean material may break down the network in a similar way that kinetoplasts are broken down by enzymes, and examine the topology of the smaller clusters that are released from the network (for example with atomic force microscopy). How might a Borromean material be distinguished from a Hopf-linked catenated network?

Chen et al. [18] discuss the probability of isolated rings as well as Hopf-linked doublets and triplets being released from kinetoplast networks during enzyme digestion, assuming different lattice geometries. The isolation probabilities depend on the linearization probability p of a minicircle being cut by the enzyme, equivalent to a node being removed from a graph, as well as the co-probability $q = 1 - p$, which is equivalent to our lattice occupation probability. We may calculate similar probabilities for Borromean connectivity on the square lattice. To find the probability of isolating a single ring from the network, we consider a 3×3 lattice with the central node occupied, and find that 34 of the 2^8 possibilities for the surrounding nodes being occupied lead to the central node being isolated. A visual demonstration of this appears in Figure 9 in the Appendix. Summing the probability of each configuration yields:

$$P_{1B} = p^4 q^5 + 8p^5 q^4 + 16p^6 q^3 + 8p^7 q^2 + p^8 q. \quad (1)$$

To find the probability of a Borromean triplet being released from the network, we consider three occupied sites in an L-shape in the center of a 4×4 grid, and find that 100 of the 2^{13} possibilities lead to the links being released. The

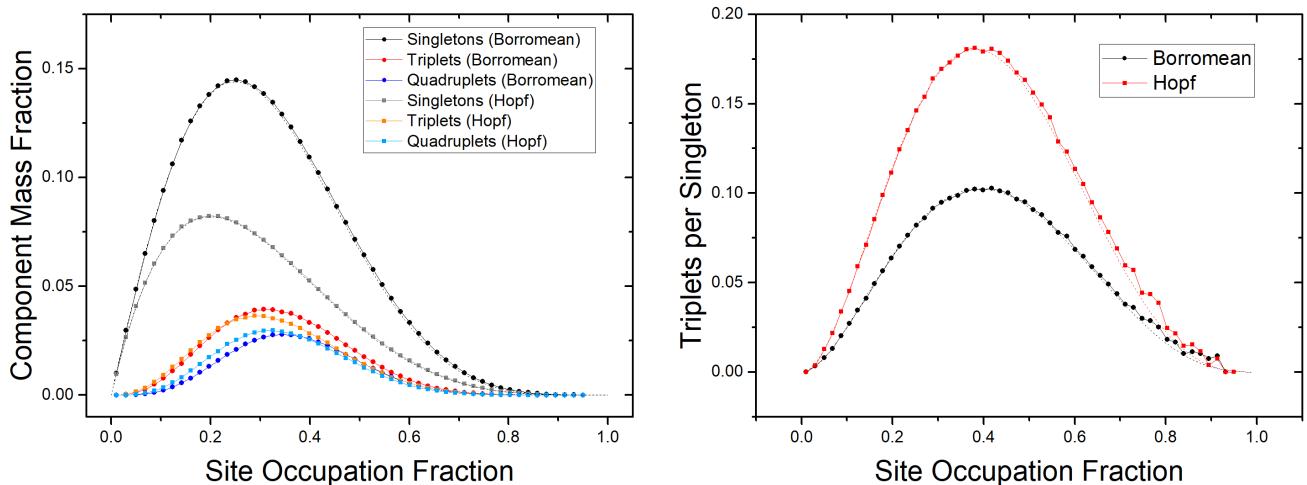


FIG. 7. Left. Fraction of total mass found in isolated loops, three-component loops, and four-component loops after a dissolution reaction of Borromean and Hopf-linked topological networks, simulated for 200x200 lattices. The exact predictions for the singlet distribution are overlaid as dotted curves, with slight discrepancies due to edge effects. Right. The ratio of triplets to singlets after a dissolution under Borromean and Hopf connectivity, with predictions overlaid as dotted curves.

total probability is:

$$P_{3B} = 4 (p^7 q^9 + 8p^8 q^8 + 24p^9 q^7 + 24p^{10} q^6 + 24p^{11} q^5 + 8p^{12} q^4 + p^{13} q^3), \quad (2)$$

the factor of 4 admitting rotations of the triplet. For comparison, the probabilities for finding an isolated component or a triplet with regular square lattice Hopf connectivity are $P_{1H} = qp^4$ and $P_{3H} = 2q^3 p^7 (2 + p)$.

Figure 7 shows the expected mass fraction of different sized components as a function of the undissolved fraction q , for Borromean and Hopf networks. A greater proportion of the mass is found in single loops under Borromean connectivity, in part due to the absence of 2-component links which occupy part of the mass in dissolved Hopf systems. There are subtle differences in the relative mass found in 3- and 4-component links between the two connectivity rules. The ratio of triplets to singlets, a parameter that could in principle be measured experimentally (and has been, for kinetoplast DNA), is shown on the right, with the ratio for Borromean networks peaking close to 20% near $q = 0.4$, but only 10% for Hopf networks. The exact expressions describe the computational data well, with some finite-size edge discrepancies at large q .

CONCLUDING REMARKS

This analysis is possible because the square lattice structure allows us to map a knot theory problem, the Borromean connection of three loops, to a graph theory problem, the continuity of connected triangles. More general linked-ring systems cannot necessarily rely on geometry to impose topology, but invariants have been derived which can detect triplet-wise Borromean connectivity when pairwise linking connectivity is absent [26]. A number of studies have used the Gauss linking number to calculate the graph structure of densely packed circles [38, 39] or ring polymers [40, 41], but the linking number cannot detect Borromean connectivity. Building upon these results, future work can examine the Borromean networks that form within dense packings once Hopf connections have been accounted for, which may be present in dense solutions of ring polymers or of DNA Olympic gels created through topoisomerase activity [7]. A topological network with both Borromean and Hopf connections between loops is suitable for analysis using hypergraphs, in which multiple degrees of connectivity may be encapsulated within the network. This analysis need not end at square lattices, nor at Borromean connectivity: networks, on- or off-lattice, may be constructed of any N -connected Brunnian link, which may present a range of percolation phenomena.

While this work is motivated by mechanically interlocked molecular networks, it may apply to any network with non-bipartite connectivity. Borromean connectivity has been discussed, for example, in the context of telecommunication

and cryptography, in which non-bipartite information transfer may be required. Notably, the Borromean ring signature has been proposed and utilized for key verification and e-voting [42–44]. As such algorithms become more widespread, an understanding of percolation phenomena in distributed key networks may prove necessary.

In summary, we have simulated the dissolution of Borromean square lattices to calculate their percolation threshold, which we find to be 2.4% higher than that of the traditional square lattice. We have also made predictions about the population of simple links released from a network during dissolution, finding marked differences from Hopf lattices due in part to the lack of Borromean dimers. Our analysis, although focusing on graph theory, makes predictions for potential future experiments to determine and verify the topology of Borromean materials [9] and understand their topology-function relationship.

ACKNOWLEDGEMENTS

The authors wish to thank Robert Ziff for his helpful discussions about percolation theory. They are also grateful to Kenny Umentum for suggesting a recursive algorithm, Raphael Candelier for his helpful blog, and Luc Devroye whose artwork inspired this project. DF is supported by the HSI-STEM Bridge to the Beach Program. This work is supported by the National Science Foundation, grant number 2105113.

-
- [1] Damien Sluysmans and J Fraser Stoddart. The burgeoning of mechanically interlocked molecules in chemistry. *Trends in Chemistry*, 1(2):185–197, 2019.
 - [2] Kelly S Chichak, Stuart J Cantrill, Anthony R Pease, Sheng-Hsien Chiu, Gareth WV Cave, Jerry L Atwood, and J Fraser Stoddart. Molecular borromean rings. *Science*, 304(5675):1308–1312, 2004.
 - [3] Nadrian C Seeman. Dna nanotechnology: novel dna constructions. *Annual review of biophysics and biomolecular structure*, 27:225, 1998.
 - [4] CA Bertulani and MS Hussein. Geometry of borromean halo nuclei. *Physical Review C*, 76(5):051602, 2007.
 - [5] Shinichi Saito and Isao Tomita. Topological carbon allotropes: knotted molecules, carbon-nano-chain, chainmails, and hopfene. *Materials Research Express*, 7(5):056301, 2020.
 - [6] José Antonio Real, Enrique Andrés, M Carmen Munoz, Miguel Julve, Thierry Granier, Azzedine Bousseksou, and François Varret. Spin crossover in a catenane supramolecular system. *Science*, 268(5208):265–267, 1995.
 - [7] Brad A Krajina, Audrey Zhu, Sarah C Heilshorn, and Andrew J Spakowitz. Active dna olympic hydrogels driven by topoisomerase activity. *Physical review letters*, 121(14):148001, 2018.
 - [8] Spencer Igram, Kenneth C Millett, and Eleni Panagiotou. Resolving critical degrees of entanglement in olympic ring systems. *Journal of Knot Theory and Its Ramifications*, 25(14):1650081, 2016.
 - [9] Flora L Thorp-Greenwood, Alexander N Kulak, and Michaele J Hardie. An infinite chainmail of m616 metallacycles featuring multiple borromean links. *Nature Chemistry*, 7(6):526–531, 2015.
 - [10] Michaele J Hardie. Self-assembled cages and capsules using cyclotrimeratrylene-type scaffolds. *Chemistry Letters*, 45(12):1336–1346, 2016.
 - [11] Luca Catalano, Luzia S Germann, Patrick A Julien, Mihails Arhangel'skis, Ivan Halasz, Krunoslav Užarević, Martin Etter, Robert E Dinnebier, Maurizio Ursini, Massimo Cametti, et al. Open versus interpenetrated: switchable supramolecular trajectories in mechanosynthesis of a halogen-bonded borromean network. *Chem*, 7(1):146–154, 2021.
 - [12] Peter Byrne, Gareth O Lloyd, and Jonathan W Steed. Guest inclusion by borromean weave coordination networks. *Journal of Coordination Chemistry*, 74(1-3):152–161, 2021.
 - [13] Michael O’Keeffe and Michael MJ Treacy. Crystallographic descriptions of regular 2-periodic weavings of threads, loops and nets. *Acta Crystallographica Section A: Foundations and Advances*, 76(2):110–120, 2020.
 - [14] Michael O’Keeffe and Michael MJ Treacy. On borromean links and related structures. *Acta Crystallographica Section A: Foundations and Advances*, 77(5):379–391, 2021.
 - [15] Luc Devroye. Wikimedia commons: Borromean chainmain tile.
 - [16] William R Wikoff, Lars Liljas, Robert L Duda, Hiro Tsuruta, Roger W Hendrix, and John E Johnson. Topologically linked protein rings in the bacteriophage hk97 capsid. *Science*, 289(5487):2129–2133, 2000.
 - [17] Theresa A Shapiro and Paul T Englund. The structure and replication of kinetoplast dna. *Annual review of microbiology*, 49(1):117–143, 1995.
 - [18] Junghuei Chen, Carol A Rauch, James H White, Paul T Englund, and Nicholas R Cozzarelli. The topology of the kinetoplast dna network. *Cell*, 80(1):61–69, 1995.
 - [19] L Ibrahim, P Liu, M Klingbeil, Y Diao, and J Arsuaga. Estimating properties of kinetoplast dna by fragmentation reactions. *Journal of Physics A: Mathematical and Theoretical*, 52(3):034001, 2018.
 - [20] David Yllanes, Sourav S Bhabesh, David R Nelson, and Mark J Bowick. Thermal crumpling of perforated two-dimensional sheets. *Nature communications*, 8(1):1–8, 2017.

- [21] Indresh Yadav, Dana Al Sulaiman, and Patrick S Doyle. Tuning the topology of a two-dimensional catenated dna network. *arXiv preprint arXiv:2209.04486*, 2022.
- [22] John W Essam. Percolation theory. *Reports on progress in physics*, 43(7):833, 1980.
- [23] Robert M Ziff. Spanning probability in 2d percolation. *Physical review letters*, 69(18):2670, 1992.
- [24] Stephan Mertens, Iwan Jensen, and Robert M Ziff. Universal features of cluster numbers in percolation. *Physical Review E*, 96(5):052119, 2017.
- [25] James Clerk Maxwell. *The Scientific Letters and Papers of James Clerk Maxwell: Volume 1, 1846-1862*, volume 3. CUP Archive, 1990.
- [26] Dennis DeTurck, Herman Gluck, Rafal Komendarczyk, Paul Melvin, Clayton Shonkwiler, and David Shea Vela-Vick. Triple linking numbers, ambiguous hopf invariants and integral formulas for three-component links. *arXiv preprint arXiv:0901.1612*, 2009.
- [27] Carlos Zapata-Carratala and Xerxes D Arsiwalla. An invitation to higher arity science. *arXiv preprint arXiv:2201.09738*, 2022.
- [28] Wai-Hung Liu and Andrew H Sherman. Comparative analysis of the cuthill–mckee and the reverse cuthill–mckee ordering algorithms for sparse matrices. *SIAM Journal on Numerical Analysis*, 13(2):198–213, 1976.
- [29] Raphael Candelier. Fast clusterization of adjacency matrices. <http://raphael.candelier.fr/?blog=Adj2cluster>.
- [30] A Margolina, HJ Herrmann, and D Stauffer. Size of largest and second largest cluster in random percolation. *Physics Letters A*, 93(2):73–75, 1982.
- [31] CR da Silva, ML Lyra, and GM Viswanathan. Largest and second largest cluster statistics at the percolation threshold of hypercubic lattices. *Physical Review E*, 66(5):056107, 2002.
- [32] Yong Zhu, Zi-Qing Yang, Xin Zhang, and Xiao-Song Chen. Critical behaviors and universality classes of percolation phase transitions on two-dimensional square lattice. *Communications in Theoretical Physics*, 64(2):231, 2015.
- [33] Jingfang Fan, Maoxin Liu, Liangsheng Li, and Xiaosong Chen. Continuous percolation phase transitions of random networks under a generalized achlioptas process. *Physical Review E*, 85(6):061110, 2012.
- [34] Robert M Ziff. Correction-to-scaling exponent for two-dimensional percolation. *Physical Review E*, 83(2):020107, 2011.
- [35] Shane Macleod and Naem Jan. Large lattice simulation of random site percolation. *International Journal of Modern Physics C*, 9(02):289–294, 1998.
- [36] Binbin Ding, Chaolin Li, Meng Zhang, Gang Lu, and Fei Ji. Numerical analysis of percolation cluster size distribution in two-dimensional and three-dimensional lattices. *The European Physical Journal B*, 87(8):1–8, 2014.
- [37] Joseph Hoshen, D Stauffer, George H Bishop, Ralph J Harrison, and George D Quinn. Monte carlo experiments on cluster size distribution in percolation. *Journal of Physics A: Mathematical and General*, 12(8):1285, 1979.
- [38] Y Diao, K Hinson, R Kaplan, M Vazquez, and J Arsuaga. The effects of density on the topological structure of the mitochondrial dna from trypanosomes. *Journal of mathematical biology*, 64(6):1087–1108, 2012.
- [39] V Rodriguez, Y Diao, and J Arsuaga. Percolation phenomena in disordered topological networks. In *Journal of Physics: Conference Series*, volume 454, page 012070. IOP Publishing, 2013.
- [40] Davide Michieletto, Davide Marenduzzo, and Enzo Orlandini. Is the kinetoplast dna a percolating network of linked rings at its critical point? *Physical biology*, 12(3):036001, 2015.
- [41] Giuseppe D’Adamo, E Orlandini, and Cristian Micheletti. Linking of ring polymers in slit-like confinement. *Macromolecules*, 50(4):1713–1718, 2017.
- [42] Gregory Maxwell and Andrew Poelstra. Borromean ring signatures. *GitHub*, 2015.
- [43] Shubhani Aggarwal and Neeraj Kumar. Signature primitives. In *Advances in Computers*, volume 121, pages 109–121. Elsevier, 2021.
- [44] Licheng Wang, Xiaoying Shen, Jing Li, Jun Shao, and Yixian Yang. Cryptographic primitives in blockchains. *Journal of Network and Computer Applications*, 127:43–58, 2019.

APPENDIX

For completeness, we present results for the second-largest component of Borromean lattices that correspond to Figure 1, in which red and green loops share Borromean links with each other mediated by yellow or blue loops, but blue and yellow loops do not share Borromean links mediated by red or green loops. Compared to the generalized lattice mapping we describe in the main text, this version breaks translational symmetry. To count connectivity between between sites, green and red sites must form a triangle with one nearest neighbor and one next-nearest neighbor, while blue and yellow sites must form a triangle with two nearest neighbors. As can be seen from Figure 7, the deviation from the square lattice is stronger, with the percolation threshold occurring at approximately $q = 0.66$.

Figure 9 depicts 3x3 grids with the center square filled, and the ten unique ways that the surrounding squares can be filled without binding the central square into a Borromean link. With the black squares occupied with probability q and the white squares with probability $p=1-q$, each grid contributes $q^m p^n$ to the probability of a single square being unbound. Most of the configurations have degeneracy due to rotation and reflection, which contribute to the total singleton probability.

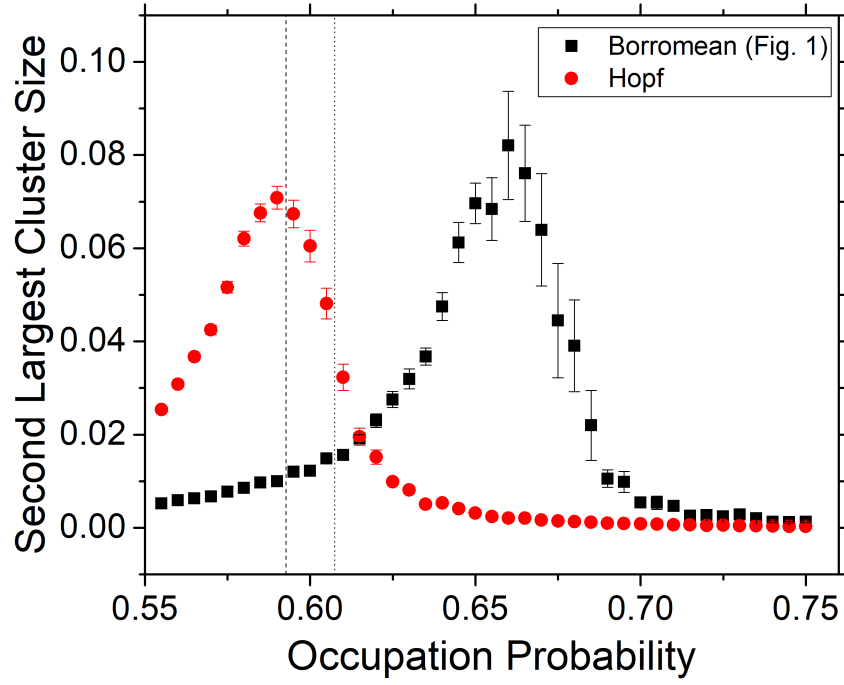


FIG. 8. The second largest component size for 200×200 square lattices corresponding to the network in Figure 1a. The vertical lines are at 0.5927 and 0.6075, the percolation thresholds for traditional square lattice connectivity, and fully symmetric Borromean square lattice connectivity. The peak is located close to 0.66.

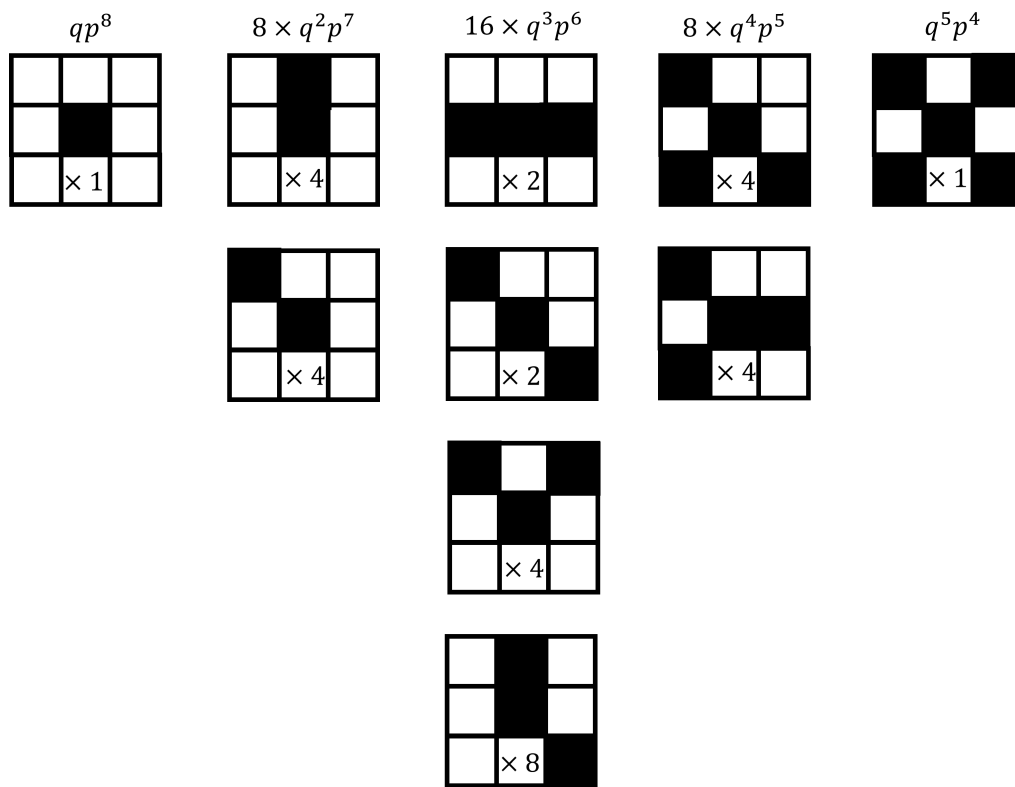


FIG. 9. A visual derivation of Equation 1, showing the ten unique 9x9 grids that will release the central occupied square. The numbers in each grid indicates their degeneracy under rotations and reflections, and the expressions on top indicate the contribution of that column to the total probability of a singleton being released.